LASER & PHOTONICS REVIEWS

www.lpr-journal.org

Strong and Omnidirectional Light Absorption from Ultraviolet to Near-Infrared Using GST Metasurface

Chensheng Li, Ruhao Pan, Guangzhou Geng, Ruixuan Zheng, Changzhi Gu, Haiming Guo, and Junjie Li**

For the perfect light absorber, it has been a huge challenge to simultaneously realize ultra-broadband and strong absorption of unpolarized light over a large angular range, though various materials and designs have been tried. The emergence of optical metasurface with powerful light field regulation ability provides a promising new strategy for achieving perfect absorbers. Here, a $Ge_2Sb_2Te_5$ (GST)-based metasurface with an average 92.5%/94.7% (experiment/simulation) absorptivity of unpolarized light, covering an ultra-broadband from ultraviolet to near-infrared region is designed and demonstrated. This GST-based metasurface consists of double-layer GST interspaced by SiO_2 layer, and both field localizations in the top patterned GST layer and intrinsic loss of the bottom patternless GST layer together contribute to this broadband absorption over wide incident angles up to 70°. Strong absorbing ability, large angular responses, and feasibly scalable fabrication for such a perfect GST-based metasurface absorber offer more promising application opportunities in integrated optoelectronic devices.

1. Introduction

Ideal electromagnetic wave absorbers possess nearly perfect absorption for omnidirectional and unpolarized incident radiation over a certain waveband, which can also be called blackbody absorbers, showing extremely valuable applications in solar photovoltaics, cloaking, photodetection, photocatalysis, and optical modulators.[1–9] Great efforts have been made to achieve perfect absorbers. Nowadays, blackbody absorbers are usually coated layers composed of different nanomaterials and nanostructures, such as vertically aligned carbon nanotube forest,[10–12] silicon nanocone,[2] oxide nanorods,[13] various metallic nanostructures,[14,15] and so on. Notably, metasurfaces, which are artificial sub-wavelength structures with tailored optical responses, come to be good candidates for perfect absorbers in recent years. And perfect absorbers composed of metasurface have been widely studied for their superiorities of easy integration, ultra-thin thickness, and high performance in controlling light field.[16–19] Metasurface perfect absorbers (MSPAs) usually adopt a sandwich-like configuration, where the three layers are metallic patterns, dielectric spacers, and metallic layer from top to bottom.[20] Moreover, the originally reported MSPAs mostly work at a single wavelength in the low-frequency band,[16] which limits their practical applications. Thus, many attempts have been implemented to broaden the absorption bandwidth as well as increase response frequency. The response frequency can be increased by shrinking the feature sizes of the unit cell. There are mainly two approaches to broaden the absorption band, including overlapping the absorption peaks and lowering the quality factor of resonance.[21–29] In order to achieve the aims above, various configurations such as Multilayer structure, plasmonic nanoparticles, and gradual size unit cells have been considered and achieved some meaningful results.[22–25,30] Several novel strategies such as utilizing dispersion compensation and nonresonant effects proposed by Fan et al. are also promising to obtain broadband absorption response.[31] Besides, the material is another key that can affect the performance of the absorber. Phase change materials have been demonstrated to achieve active absorbers based on the distinction of resonant mode between dielectric and metallic phases.[32,33] Apart from the conventional metals and dielectrics, TiN, ITO, and even black phosphorus have also been used to build up wideband MSPAs.[34–37] Furthermore, graphene-based metasurfaces are supposed to achieve ultra-broadband absorption in recent years and have been demonstrated with ≈85% absorptivity over an ultra-wide operating band that ranges from ultraviolet (UV) to near-infrared (NIR).[38] So far, however, the MSPAs still can hardly achieve the ultra-wide operating band and relatively high absorptivity (>90%) at the same time due to the limitation of the complex fabrication, configuration design,

C. Li, R. Pan, G. Geng, R. Zheng, C. Gu, H. Guo, J. Li
Beijing National Laboratory for Condensed Matter Physics
Institute of Physics
Chinese Academy of Sciences
Beijing 100190, China
E-mail: hmguo@iphy.ac.cn; jjli@iphy.ac.cn

C. Li, R. Zheng, C. Gu, H. Guo, J. Li
School of Physical Sciences
CAS Key Laboratory of Vacuum Physics
University of Chinese Academy of Sciences
Beijing 100049, China

J. Li
Songshan Lake Materials Laboratory
Dongguan, Guangdong 523808, China

The ORCID identification number(s) for the author(s) of this article can be found under https://doi.org/10.1002/lpor.202200364

DOI: 10.1002/lpor.202200364

and material selection. For example, due to the stoichiometry and phase inhomogeneity during the deposition process, the accurate fabrication of TiN is not easy to implement, and thus the practical application is limited.[39] Consequently, new materials and configurations need to be developed to realize the ultra-wideband, perfect absorption.

Materials with high loss are popular in designing perfect absorbers. $Ge_2Sb_2Te_5$ (GST) is one of the well-established phase-change materials with promising applications in rewriteable optical data storage and non-volatile electronic memory.[40] Notably, GST has a large imaginary part of dielectric permittivity (i. e. large extinction coefficient) in the visible (VIS) region, which means it is a high-loss material. Thus, GST is more easily to achieve high absorption metasurfaces based on its intrinsic light loss. The previous report has simulated and demonstrated that a GST layer introduced between the Au metasurfaces layer and the bottom mirror can achieve broadband, wide incident angle, and polarization-independent light absorption in the VIS regime,[41] but the experimental realization of such structure still lacks. On the other hand, GST mainly participates in the metasurface to modulate the electromagnetic waves only as a spacer layer, and its strengths are not well exploited. Thus, the metasurface absorbers based on the GST unit cells are expected to have the potential to realize both ultra-broadband and strong absorption, but no related results have been reported at present.

In this paper, we design and experimentally demonstrate a polarization-independent GST-based MSPA with an ultra-broad absorption band covering from UV to NIR region over a wide incident angle. The MSPA is composed of four layers, where from the bottom to the top are Cr layer, patternless GST film, SiO_2 spacer, and an array of GST nanostructure that consists of a nanocross together with four nanodisks. Each key feature size has been optimized by the finite domain time difference (FDTD) method, and perfect absorption has been observed over an ultra-broadband range from 250 to 1000 nm. Near field electric field distribution proves that the absorption effect origins from the combined action of the plasmonic coupling between the nanostructures, the electric dipole of the nanocross, and the intrinsic loss of GST. Both physical/chemical vapor deposition and electron beam lithography (EBL) are used to fabricate the metasurface bottom up. The optimized absorber achieves a measured average absorptivity of 92.5% among the operating band, which is in good agreement with the simulated results (94.7%). The strong absorption of the MSPA can maintain when the incident direction is tilted, an average absorptivity that over 77% can also be found for the glancing angle being up to 70°. In addition, the as-designed MSPA possesses tetragonal symmetry, which in turn results in the polarization independence, meaning that the MSPA has a high absorption performance even for the natural light. The realization of the GST-based MSPA provides a promising way for perfect absorbers with low material cost and opens up a horizon for integrated optoelectronic devices.

2. Results and Discussion

2.1. Design and Simulations

The proposed GST-based MSPA consists of four layers, among which the top GST layer is patterned as a metasurface structure, as shown in **Figure 1**a. A silicon substrate with 2 cm × 2 cm in area was selected to support the upper layers. The Cr film was chosen as the ground layer, which can reflect the light and block light transmission due to its low cost, which can also be substituted by Ag.[19,38] The three upper layers form a sandwich structure and dominate the absorption of incident light. The top GST layer is patterned by an array of unit cells with a nanocross and four nanodisks, possessing tetragonal symmetry so as to obtain polarization-independent absorption. The bottom GST layer without any pattern is separated from the top layer by the SiO_2 spacer layer. All the geometric parameters are shown in Figure 1b, where the length and linewidth of the nanocross are $L = 650$ nm and $w = 70$ nm, and the radius of the nanodisk is labeled as r, whose center to the edge of the nanocross is $d = 145$ nm. The unit cells are periodically arranged along x–axis and y–axis with $P = 750$ nm, and the thickness of each layer are $h_1 = 130$ nm, $h_2 = 50$ nm, $h_3 = 170$ nm and $h_4 = 30$ nm, respectively. Figure 1c depicts the refractive index and extinction coefficient of amorphous GST, clearly showing a large extinction coefficient from the UV to NIR range, which would result in a high intrinsic loss and thus provide a good cornerstone for MSPA. Here, amorphous GST is used in the following work because it has batter broadband absorptivity than crystalline GST, which will be also demonstrated in the behind.

The absorption spectra of various structures have been simulated by the FDTD method to optimize the configurations of the GST-based metasurface, and the simulated results of various structures are displayed in **Figure 2**. Due to the transmission light being blocked by Cr layer, the absorptivity can be calculated by $A = 1\text{-}R$, where R indicates the reflection and can be obtained from simulation. Figure 2a shows the configuration optimization process of the GST-based absorber along the red arrow. The absorption performance is improved step by step, and the corresponding simulated spectra are exhibited in Figure 2b. First, Cr/GST layers are chosen as the initial component without any optimization. Thanks to the intrinsic loss of the GST, although there are still ways to the perfect absorption, the absorptivity of higher than 60% at the corresponding band can be acquired. In order to further enhance the absorptive performance, a SiO_2 layer of 50 nm in thickness is coated on the GST layer, which acts as an anti-reflection layer.[34] Compared to Cr/GST layer, the absorption in the UV region has dramatically increased to 95%, but the absorptivity still drops rapidly above 880 nm. Then, the second GST layer is covered on the top to build a multilayer structure. Although the absorption in the infrared region is enhanced, the patternless GST layer lowers the absorption of the UV band no matter how thick the GST layer is (Figure S1, Supporting Information). Thus, the results are still unsatisfactory. Therefore, a cross-shaped GST resonator is introduced to replace the patternless GST layer, which was widely used in the perfect absorber.[18,42] The addition of cross-shaped GST resonator improves the absorptivity compared to multilayer, apart from the VIS band, the perfect absorptivity at UV and partial NIR region has been reached. On that basis, we proposed appending four nanodisks around the nanocross, which exhibits near-unity high absorption from 200 to 1000 nm. Figure 2c depicts the nanodisk radius dependence of absorption spectrum. A large proportion of area exceeds 90% in

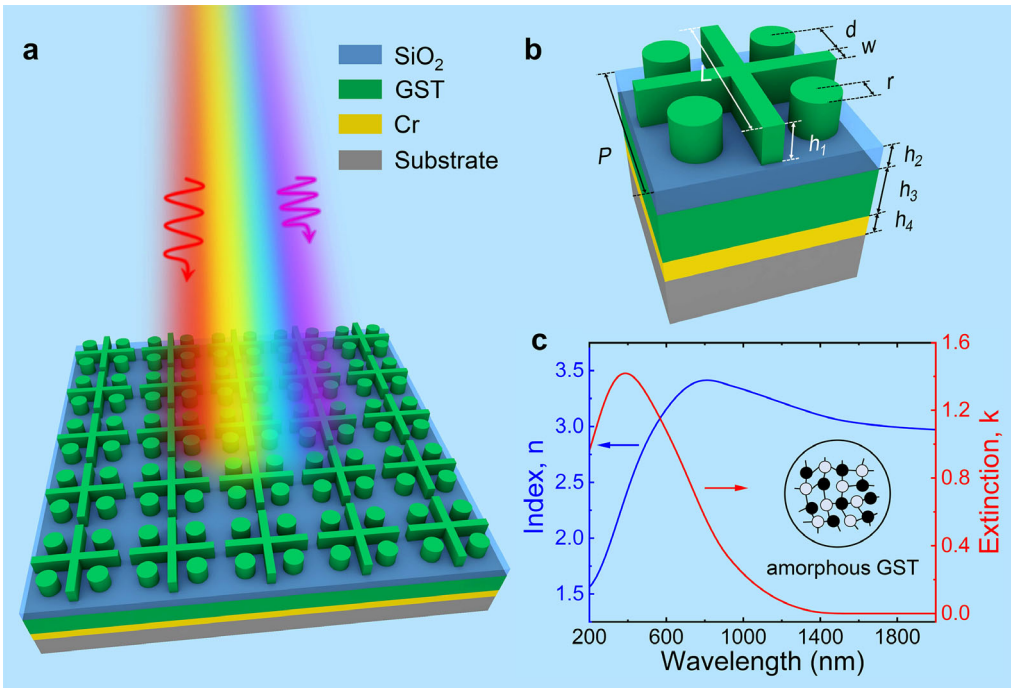

Figure 1. Schematic of designed GST-based metasurface and optical parameter of GST. a) Schematic illustration of GST-based MSPA with the capability of absorbing broadband unpolarized light. b) Schematic of a unit cell of the metasurface, identifying the structural geometric parameters. c) Wavelength dependence of refractive index and extinction coefficient for amorphous GST.

absorptivity, demonstrating the rationality and the robustness of the proposed structure. According to the analysis results in Figure 2d, the average absorptivity realizes the maximum value when the radius of nanodisk set as 80 nm, which reaches 94.5% and 91.1% for spectral range from 200 to 1000 nm and 200 to 1300 nm, respectively. The absorptivity versus incident angle and wavelength of the optimal configuration for incident light with different polarization states are shown in Figure 2e–g. The absorptivity of TE-polarized and TM-polarized light exhibit rare distinctions and both can maintain high with the increase of incident angle, leading to strong absorption for unpolarized incident light over a wide angular range. Therefore, the optimized configuration of GST-based MSPA is obtained to possess ultra-broadband, strong, omnidirectional, and polarization-independent absorption in the simulation. In addition, for above optimized configuration of GST-based MSPA, the simulated absorption result of amorphous GST is compared with that of crystalline GST, as shown in Figure S2, Supporting Information. We can see that amorphous GST's broadband absorptivity is better than that of crystalline GST, so amorphous GST is used in the following experiments. Thermal stability of the absorber is one issue regarding to the phase transition effect of GST. From our simulated results in Figure S2, Supporting Information, we found that even though the temperature rose above 160 °C, the absorptivity of crystalline GST metasurface absorber only had a slight decrease and still maintain a relatively high level. This result indicates a nice thermal stability of the GST metasurface absorber, which is very useful for its potential application at high temperature.

2.2. Fabrication Process

After the optimized structure has been built up, a nanofabrication process has been developed for the GST-based MSPA. **Figure 3**a shows the illustration of the fabrication process for GST-based MSPA. The fabrication process starts from Cr layer deposition on silicon substrate by electron beam evaporation (EBE). After that, the GST and SiO_2 film with 170 and 50 nm in thickness were grown by magnetron sputtering (MS) and inductively coupled plasma enhanced chemical vapor deposition (ICPECVD), respectively. Then, the photoresist was spin-coated on the SiO_2 layer, and an array of nanopatterns of optimized unit cell was directed written by EBL. After the pattern development, MS method was applied again to deposit GST film. After the lift-off process, the patterned GST was taken shape to form the whole GST-based MSPA finally. During MSPA fabrication process, all the GST remained amorphous GST, which was verified by X-ray diffraction (XRD) measurement (Figure S3, Supporting Information).

Figure 3b shows an optical photograph of the fabricated sample, where the 1 cm × 1 cm dark area indicates the perfect absorber, showing the capability of large-area fabrication. Figure 3c demonstrates a tilted scanning electron microscope (SEM) view of the sample of MSPA, where excellent uniformity of the unit cell proves that the developed fabrication process is an effective fabrication method. A magnifying SEM image in Figure 3d further exhibits the GST structure in the array has consistent sizes with the simulated one. The SEM image of cross-sectional profile of Cr/GST/SiO_2 layer is also given in Figure S4, Supporting

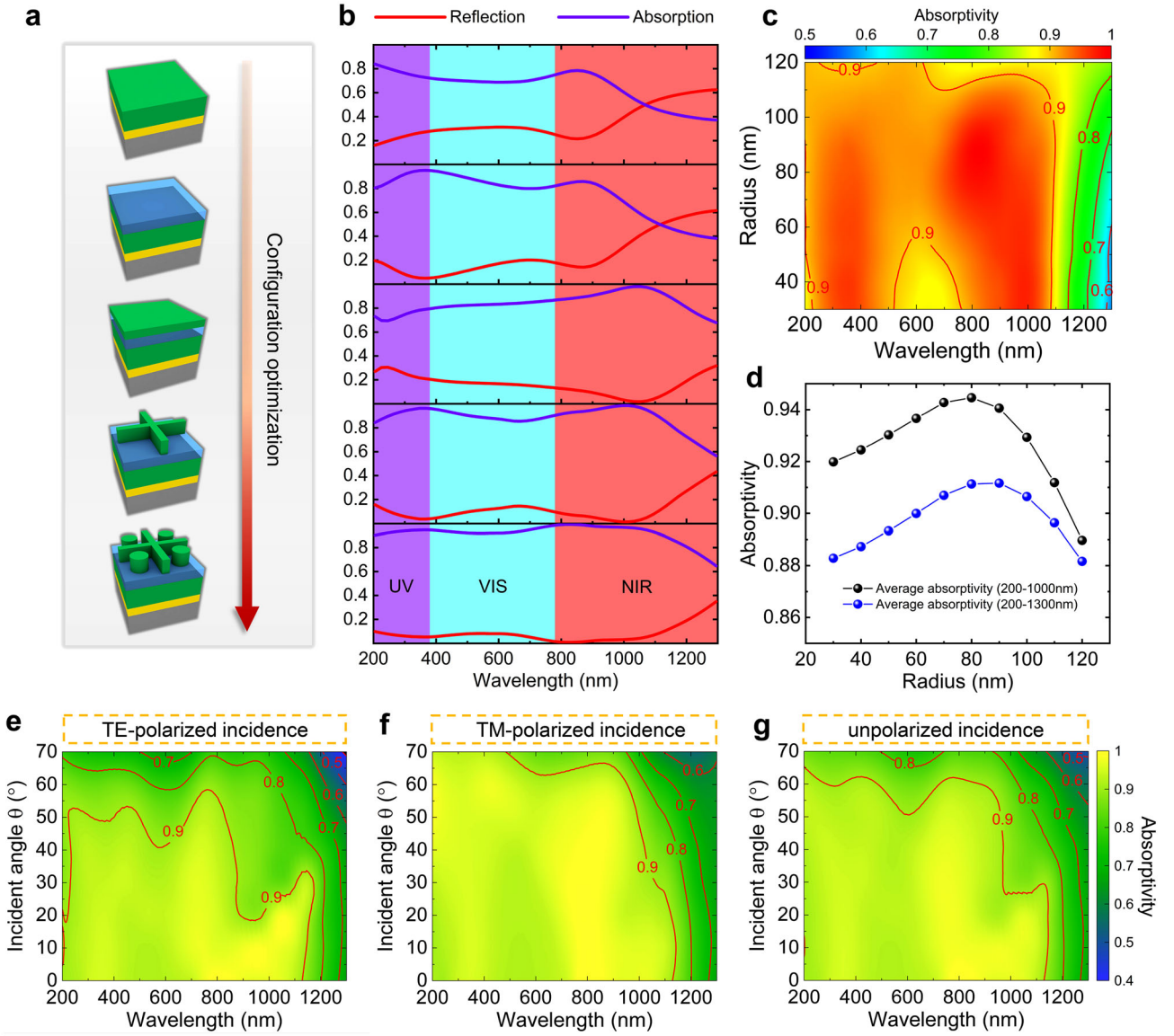

Figure 2. Configuration-optimized scheme and simulation results. a) Schematic for the configuration optimization process, in which from top to bottom are Cr/GST layers, Cr/GST/SiO_2 layers, Cr/GST/SiO_2/GST layers, Cr/GST/SiO_2 layers/GST metasurface containing nanocrosses, and Cr/GST/SiO_2 films/GST metasurface containing nanocrosses and nanodisks. b) Simulated absorption spectra with corresponding to the related structure in a) one by one. c) Absorptivity versus nanodisk radius and wavelength for the GST-based MSPA. d) Nanodisk radius dependence of average absorptivity for different spectrum ranges. Simulated absorptivity map versus incident angle and wavelength for e) TE, f) TM, and g) unpolarized light.

Information to show the thicknesses of each layer. Figure 3e illustrates an optical microscope image of the logo of Institute of Physics CAS made of the perfect absorber. The black area of the logo indicates this method is suitable for the patterned fabrication.

2.3. Measurement Results

In order to verify the performance of the GST-based MSPA, we characterized the absorptivity spectra from 250 to 1300 nm. Since the transmission light is blocked, the absorptivity was determined by $A = 1\text{-}R$. **Figure 4**a shows the measured results of the GST-based MSPA for unpolarized incident light (blue curve). Furthermore, the average absorptivity within various spectrum ranges is extracted and displayed in Figure 4b. It can be seen that the measured absorptivity exceeds 94% and can be up to 97% even in the entire UV band. In detail, the average absorptivity is capable of achieving 95.6%. In the VIS band, the absorptivity marginally decreases with the increase of incident wavelength, and the average of 97.7% and 91.4% were obtained for 380–550 nm and 550–780 nm regions, respectively, confirming the excellent absorption ability of our perfect absorber. Furthermore, the absorptivity maintains 87% when the wavelength of the incident light rises to 1000 nm and the average absorptivity within 780–1000 nm is 87%, demonstrating the GST MSPA

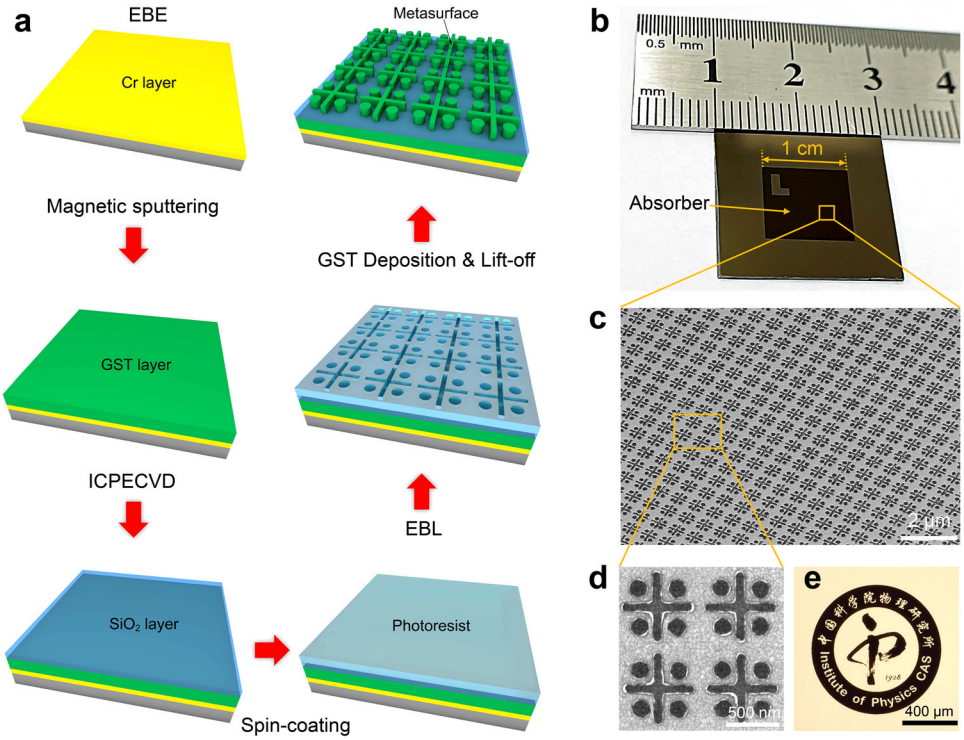

Figure 3. Fabrication process and the morphology of GST-based MSPA. a) Schematic diagram of the fabrication process of GST-based MSPA. b) Photograph of as-fabricated MSPA with 1 cm × 1 cm area. c) Tilted SEM image of the large area GST nanostructure array. d) Partial detailed SEM image of the unit cell. e) Optical microscope image of the logo of the Institute of Physics CAS, and the black area of the logo indicates the absorber.

is capable of absorbing a part of NIR light. The average absorptivity from 250 nm to 1000 nm is 92.5%, which is very close to the simulation result (94.7%). Besides, we also measured the absorptivity of the structure without the top patterned GST layer (green curve), as shown in Figure 4a. It is obvious that the absorption ability of Cr/GST/SiO_2 layers structure is poor than the MSPA, indicating the top patterned layer has an important effect on light absorption. In addition, we note that the absorptivity fluctuates slightly with the change of wavelength within the absorption band, which will lead to a situation where some measured absorptivities are slightly higher or lower than the FDTD simulated ones. However, from the whole absorption band view (≈250–1000 nm), the measured average absorptivity (92.5%) is still lower than FDTD simulated ones (94.7%), which is reasonable. The deviation between measurement and simulation comes mainly from the errors in sample fabrication processes.

To clarify this issue and investigated the distribution status of light absorption, we calculated the absorbed electromagnetic power using a simple formula $P_{abs} = 1/2\omega\varepsilon''|E|^2$, where ω is the angular frequency, ε'' is the imaginary part of the dielectric permittivity, and $|E|$ is the total electric field in the material, and the calculated result is plotted in Figure 4c. As we can see, the top patterned GST layer plays a crucial role in the MSPA, which absorbs the majority of the incident light. With the increase of wavelength above 1000 nm, the contribution of the top layer decreases rapidly. There are totally two reasons to explain this behavior: First, as shown in Figure 1c, the extinction coefficient of GST becomes low above 1000 nm, resulting in relatively low light loss. Second, the wavelength of light in this region is far larger than the feature size of the nanostructure, which exceeds the manipulation scope of the metasurface. In addition, more incident light transmits the top layer, causing an increasing contribution of the underneath GST layer with wavelength increase. In summary, the top GST layer with nanostructures combined with the compensation of underneath patternless GST layer yield an excellent perfect absorption effect. The absorptivity spectra indicate that the GST-based MSPA can efficiently absorb the unpolarized incident light from 250 to 1000 nm. Our device possesses a rather broad absorption band and high absorptivity compared with previous works.[19,30,34]

To understand the absorption mechanism of the top GST layer with nanostructures, we analyzed the electrical field distribution in the structure with x-polarized incident light. Figure 4d shows the cross-section of the nanocross resonator and the corresponding electric field intensity profile along the x–y plane with z = 370 nm at wavelengths of 350, 750, and 900 nm. The electric field is localized along the surface of the cross along y–axis at 350 nm, indicating the dipole resonance is motivated, which causes loss and therefore improves the absorptivity compared to the multilayer structure.[43] For the wavelengths of 900 nm, the dipole resonance transfers to the ends of the cross along x–axis. A similar circumstance happens for the structure of cross and four nanodisks (z = 370 nm), as shown in Figure 4f, in which the dipole resonances exist around the nanodisks along x–axis at 350 nm as well. Notably, as depicted in the middle column of Figure 4e,f, the nanodisks couple with the nanocross at 750 nm, and the electric field is localized between the gaps along x–axis. The field localizations cause the surface localized field coupling into the material,

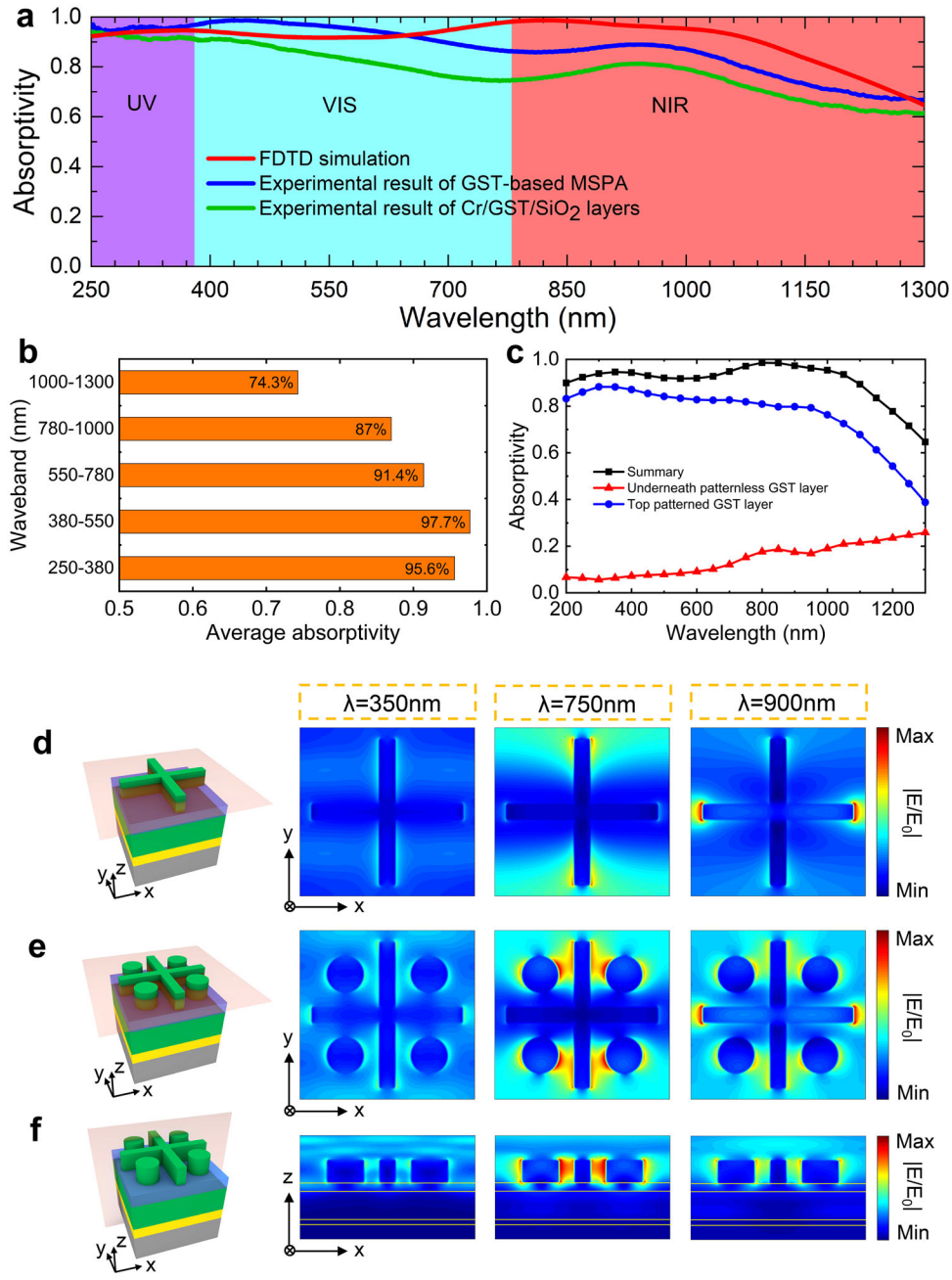

Figure 4. Measured absorption spectra of GST-based MSPA and the electric field distribution profile. a) Measured absorption spectra of the GST-based MSPA for unpolarized light incidence from 250 to 1300 nm, the blue curve indicates the absorption spectra of MSPA, and the green curve denotes the sample without top patterned GST nanostructure. The simulation result (red curve) is also shown for comparison. b) The average absorptivity of various spectral regions from UV to NIR. c) Calculated absorption contribution for the top GST metasurface layer and the underneath patternless GST layer. d–f) Schematic illustration of cross-sections and the corresponding electric field distribution profile maps at three selected incident light wavelengths: 350, 750, and 900 nm.

compensating for the deficiency of the cross-shaped pattern and further enhancing the absorptivity in the visible region. Thus, an ultra-broadband perfect absorption can be achieved. The electric field intensity in the underneath GST layer increases continuously with wavelength from 350 to 750 nm and then to 900 nm, as shown in Figure S5, Supporting Information, which is corresponding to the trend of absorption contribution of underneath GST layer. Consequently, the intrinsic loss of patternless GST layer together with the field localizations in patterned GST layer caused by dipole resonance and the coupling between nanostructures result in the broad absorption band of our device.

In addition, absorption spectra of GST-based MSPA for unpolarized light with varying incident angles are collected, demonstrating its omnidirectional perfect absorption ability. **Figure 5**a

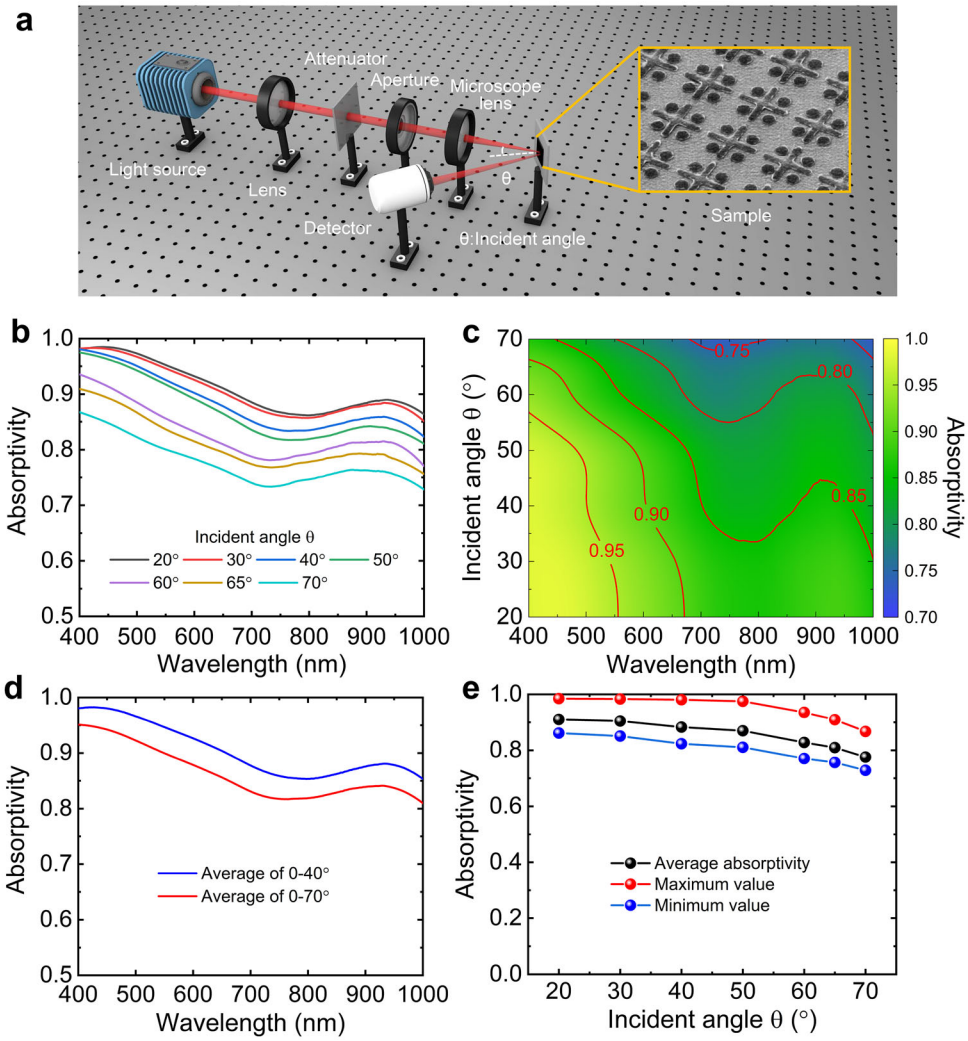

Figure 5. Measured absorptivity spectra for unpolarized light with varying incident angles. a) Schematic diagram of the optical setup for angle-varying incidence. b) Incident light wavelength dependence of absorptivity under various incident angles. c) Absorptivity versus incident angle and wavelength for the metasurface. d) The average value of absorptivity from 0° to 40° (blue curve) and 0° to 70° (red curve), respectively. e) Average, maximum and minimum absorptivity from 400 to 1000 nm under certain incident angles.

exhibits the optical setup for the angle-varying measurement. A glancing angle of θ both for the incident and reflected beam is introduced to determine the reflectivity of the MSPA, where the unpolarized light was focused on the vertically placed sample by lens and aperture. The measured results are shown in Figure 5b, from which we can see that the absorptivity decrease gradually but remains high with the incident angle changes from 20° to 70°. An absorptivity map versus incident angle and wavelength for the absorber have drawn in Figure 5c, which can present the strong absorption more intuitional. According to the measurements, average absorption spectra from 0° to 40° and 0° to 70° are depicted in Figure 5d, indicating that the incident angle has a small impact on the absorption ability of the MSPA. Figure 5e shows the average absorptivity from 400 to 1000 nm under certain incident angles, which drops slowly and maintains a relatively high value with the increase of incident angle. From the result, we obtained that the average absorptivity exceeds 77% even at the glancing angle increased to 70°. The incident angle dependence of maximum and minimum values of the absorptivity is shown as well, suggesting the high uniformity of light absorption. We could conclude from the above experimental results that our device possesses an omnidirectional property and can absorb the unpolarized incident light at wide angles.

A comparison of our proposed broadband MSPA with previous reports is summarized in **Table 1**, showing a very good competitivity in overall performance of our MSPA. In the next works, both absorption efficiency and bandwidth for our GST-based MSPA are hopefully being further improved and widened through some feasible approaches, such as the configuration optimization and combination with graphene. In addition, it is worth noting that active GST-based MSPAs are more attractive but it can be only realized within a certain narrow waveband up to now,[44] while achieving broadband tunable devices remains a challenge. Thus, further efforts deserve to be made to achieve this goal utilizing an improved GST metasurface structure.

Table 1. Comparison of as-proposed broadband MSPA in this work with available literatures.

Major material	Absorption waveband	Operating bandwidth	Average absorptivity	Number of layers	Polarization independent	References
Ag	VIS	300 nm	71%	3	Yes	Ref. [19]
Cr	VIS–NIR	800 nm	>90%	3	Yes	Ref. [24]
Au	UV–VIS	400 nm	>94%	2	Yes	Ref. [25]
Cr、Si	VIS	360 nm	95.8%	2	Yes	Ref. [26]
Au、SiO_2	VIS	350 nm	>95%	3	Yes	Ref. [30]
TiN	VIS–NIR	400 nm	95%	3	Yes	Ref. [34]
TiN、Ti	VIS–NIR	1645 nm	>99%	6	Yes	Ref. [37]
Graphene	UV–NIR	2200 nm	<90%	≈32	Yes	Ref. [38]
GST	UV–NIR	750 nm	92.5%	4	Yes	This work

3. Conclusion

In conclusion, we design and experimentally demonstrate a GST-based MSPA with ultra-broadband and strong absorption ability. An array of tetragonal symmetric GST-nanostructures on the top layer plays a key role in these MSPAs. Near field distribution shows the intrinsic loss of GST as well as the field localizations caused by dipole resonance and the coupling between nanostructures, resulting in a broad perfect absorption band ranging from UV to NIR. High absorption can maintain even at the incident angle up to 70°, and the highest average absorptivity of 92.5% is obtained from 250 to 1000 nm. Such GST-based MSPA in our work can achieve the ultra-wide operating band and relatively high absorptivity (>90%) at the same time, providing a good demonstration of an ideal light absorber. In particular, the feasible configuration and scalable fabrication for our GST-based MSPA will enable more applications in various advanced optoelectronic devices.

4. Experimental Section

Fabrications: An intrinsic silicon wafer acting as the substrate was chosen. Before fabrication, a 2 cm × 2 cm silicon substrate was ultrasonically cleaned in acetone, isopropanol, and ultrapure water, and subsequently dried with nitrogen flow. The fabrication process consisted of six steps. First, the 30 nm Cr layer was deposited on the substrate by EBE (FU-12PEB). Then, an amorphous GST layer with a thickness of 170 nm was deposited by MS method (Combo-1220). The deposition of GST was performed using a synthesized single target at room temperature with argon gas flow rate at 10 sccm, growth pressure at 0.007 mTorr, and sputtering RF power of 100 W. After that, the 50 nm thickness SiO_2 layer was grown by ICPECVD (SI 500D). Then, polymethyl methacrylate (PMMA 495 K) with 300 nm in thickness was spin-coated at 2000 rpm and pre-baked for hardening as the resist. For the sake of preventing GST phase change, the sample was baked at 95 °C for 30 min, which was below the phase change temperature of amorphous GST (160 °C). Afterward, The PMMA was exposed by EBL (EBPG 5200, Raith) and thus the pattern was obtained after development. Finally, GST was further deposited by MS method, and a lift-off process performed ultrasonically in acetone was carried out to remove needless materials out of patterns.

FDTD Simulations: The reflection, transmission, and electric field profiles of the MSPA were simulated using the FDTD method. A mesh size of 5 nm along all directions and a mesh accuracy of 4 were used. The 3D model of the unit cell was built up and simulated with periodic boundary conditions along the *x*–axis and *y*–axis and perfectly matched layers (PML) along the propagation of electromagnetic waves (*z*–axis). Plane waves were launched incident to the unit cell along –*z* direction.

Measurements: A homemade optical test platform was introduced to collect the reflective spectra of the metasurface. During the test, the source light was focused on the MSPA by a 10× objective with a numerical aperture of 0.25, and several spectrometers (HR2000+ES, PG 2000, NIR 1700) were used to collect the reflective signal. Due to the extremely high reflection, the reflection signal of Ag and Al mirrors was used as the reference for VIS–NIR and UV regions, respectively. The absorptive spectra were then obtained by $A = 1\text{-}R$, since the Cr layer prevents light transmission. The SEM photographs were taken on Hitachi Regulus 8230 with an acceleration voltage of 25 KV. The refractive index and extinction coefficient of GST were measured on a spectral ellipsometry (SE 850 DUV). The XRD measurement was performed using a PAN-analytical X-ray diffractometer with Cu K_α radiation.

Supporting Information

Supporting Information is available from the Wiley Online Library or from the author.

Acknowledgements

C.L. and R.P. contributed equally to this work. This work was supported by the National Natural Science Foundation of China (Grant No. 12074420, U21A20140, 61888102, and 61905274), the Beijing Municipal Science & Technology Commission, Administrative Commission of Zhongguancun Science Park (No. Z211100004821009), the Chinese Academy of Sciences through the Project for Young Scientists in Basic Research (YSBR-021), and the Key Research Program of Frontier Sciences of Chinese Academy of Sciences (Grant No. QYZDJ-SSWSLH042 and XDPB22). This work was also supported by the Synergic Extreme Condition User Facility, China.

Conflict of Interest

The authors declare no conflict of interest.

Data Availability Statement

The data that support the findings of this study are available from the corresponding author upon reasonable request.

Keywords

$Ge_2Sb_2Te_5$, metasurfaces, omnidirectional absorption, polarization-independence, ultra-broadband perfect absorbers

Received: May 20, 2022
Revised: August 16, 2022
Published online:

[1] J. B. Chou, Y. X. Yeng, Y. E. Lee, A. Lenert, V. Rinnerbauer, I. Celanovic, M. Soljacic, N. X. Fang, E. N. Wang, S. G. Kim, *Adv. Mater.* **2014**, *26*, 8041.
[2] S. Jeong, M. D. Mcgehee, Y. Cui, *Nat. Commun.* **2013**, *4*, 2950.
[3] H. Shi, J. G. Ok, H. Won Baac, L. Jay Guo, *Appl. Phys. Lett.* **2011**, *99*, 211103.
[4] S. C. Song, Q. Chen, L. Jin, F. H. Sun, *Nanoscale* **2013**, *5*, 9615.
[5] W. Li, J. Valentine, *Nano Lett.* **2014**, *14*, 3510.
[6] K. T. Lin, H. L. Chen, Y. S. Lai, C. C. Yu, *Nat. Commun.* **2014**, *5*, 3288.
[7] W. Li, Z. J. Coppens, L. V. Besteiro, W. Y. Wang, A. O. Govorov, J. Valentine, *Nat. Commun.* **2015**, *6*, 8379.
[8] J. Y. Y. Loh, M. Safari, C. L. Mao, C. J. Viasus, G. V. Eleftheriades, G. A. Ozin, N. P. Kherani, *Nano Lett.* **2021**, *21*, 9124.
[9] Y. Yao, R. Shankar, M. A. Kats, Y. Song, J. Kong, M. Loncar, F. Capasso, *Nano Lett.* **2014**, *14*, 6526.
[10] K. Mizuno, J. Ishii, H. Kishida, Y. Hayamizu, S. Yasuda, D. N. Futaba, M. Yumura, K. Hata, *Proc. Natl. Acad. Sci. U. S. A.* **2009**, *106*, 6044.
[11] X. J. Wang, L. P. Wang, O. S. Adewuyi, B. A. Cola, Z. M. Zhang, *Appl. Phys. Lett.* **2010**, *97*, 163116.
[12] M. Y. Zhang, D. Y. Ban, C. Xu, J. T. W. Yeow, *ACS Nano* **2019**, *13*, 13285.
[13] R. Pietruszka, B. S. Witkowski, S. Gieraltowska, R. Caban, L. Wachnicki, E. Zielony, K. Gwozdz, P. Bieganski, E. Placzek-Popko, M. Godlewski, *Sol. Energy Mater. Sol. Cells* **2015**, *143*, 99.
[14] J. F. Huang, C. X. Liu, Y. H. Zhu, S. Masala, E. Alarousu, Y. Han, A. Fratalocchi, *Nat. Nanotechnol.* **2016**, *11*, 60.
[15] L. Zhou, Y. L. Tan, J. Y. Wang, W. C. Xu, Y. Yuan, W. S. Cai, S. N. Zhu, J. Zhu, *Nat. Photonics* **2016**, *10*, 393.
[16] N. I. Landy, S. Sajuyigbe, J. J. Mock, D. R. Smith, W. J. Padilla, *Phys. Rev. Lett.* **2008**, *100*, 207402.
[17] H. Tao, C. M. Bingham, A. C. Strikwerda, D. Pilon, D. Shrekenhamer, N. I. Landy, K. Fan, X. Zhang, W. J. Padilla, R. D. Averitt, *Phys. Rev. B* **2008**, *78*, 241103.
[18] X. Liu, T. Starr, A. F. Starr, W. J. Padilla, *Phys. Rev. Lett.* **2010**, *104*, 207403.
[19] K. Aydin, V. E. Ferry, R. M. Briggs, H. A. Atwater, *Nat. Commun.* **2011**, *2*, 517.
[20] P. Yu, L. V. Besteiro, Y. J. Huang, J. Wu, L. Fu, H. H. Tan, C. Jagadish, G. P. Wiederrecht, A. O. Govorov, Z. M. Wang, *Adv. Opt. Mater.* **2019**, *7*, 1800995.
[21] S. Butun, K. Aydin, *Opt. Express* **2014**, *22*, 19457.
[22] W. L. Guo, Y. X. Liu, T. C. Han, *Opt. Express* **2016**, *24*, 20586.
[23] Y. Cui, K. H. Fung, J. Xu, H. Ma, Y. Jin, S. He, N. X. Fang, *Nano Lett.* **2012**, *12*, 1443.
[24] M. A. Abbas, J. Kim, A. S. Rana, I. Kim, B. Rehman, Z. Ahmad, Y. Massoud, J. Seong, T. Badloe, K. Park, M. Q. Mehmood, M. Zubair, J. Rho, *Nanoscale* **2022**, *14*, 6425.
[25] H. B. Zhang, X. D. Feng, Y. F. Luo, L. Yuan, M. W. Song, Y. Y. Zhang, S. D. Jiang, Y. T. Cheng, H. Liu, *Appl. Surf. Sci.* **2022**, *584*, 152624.
[26] Q. Y. Qian, T. Sun, Y. Yan, C. H. Wang, *Adv. Opt. Mater.* **2017**, *5*, 1700064.
[27] F. Ding, Y. X. Cui, X. C. Ge, Y. Jin, S. L. He, *Appl. Phys. Lett.* **2012**, *100*, 103506.
[28] Y. Z. Cheng, Y. Wang, Y. Nie, R. Z. Gong, X. Xiong, X. Wang, *J. Appl. Phys.* **2012**, *111*, 044902.
[29] T. T. Nguyen, S. Lim, *Appl. Phys. Lett.* **2018**, *112*, 021605.
[30] M. K. Hedayati, M. Javaherirahim, B. Mozooni, R. Abdelaziz, A. Tavassolizadeh, V. S. K. Chakravadhanula, V. Zaporojtchenko, T. Strunkus, F. Faupel, M. Elbahri, *Adv. Mater.* **2011**, *23*, 5410.
[31] R. H. Fan, B. Xiong, R. W. Peng, M. Wang, *Adv. Mater.* **2020**, *32*, 1904646.
[32] J. N. Wang, B. Xiong, R. W. Peng, C. Y. Li, B. Q. Hou, C. W. Chen, Y. Liu, M. Wang, *Small* **2021**, *17*, 2101282.
[33] H. Kocer, S. Butun, B. Banar, K. Wang, S. Tongay, J. Q. Wu, K. Aydin, *Appl. Phys. Lett.* **2015**, *106*, 161104.
[34] W. Li, U. Guler, N. Kinsey, G. V. Naik, A. Boltasseva, J. G. Guan, V. M. Shalaev, A. V. Kildishev, *Adv. Mater.* **2014**, *26*, 7959.
[35] S. Shrestha, Y. Wang, A. C. Overvig, M. Lu, A. Stein, L. Dal Negro, N. F. Yu, *ACS Photonics* **2018**, *5*, 3526.
[36] J. Wang, Y. Jiang, *Opt. Express* **2017**, *25*, 5206.
[37] F. Qin, X. F. Chen, Z. Yi, W. T. Yao, H. Yang, Y. J. Tang, Y. Yi, H. L. Li, Y. G. Yi, *Sol. Energy Mater. Sol. Cells* **2020**, *211*, 110535.
[38] H. Lin, B. C. P. Sturmberg, K.-T. Lin, Y. Yang, X. Zheng, T. K. Chong, C. M. De Sterke, B. Jia, *Nat. Photonics* **2019**, *13*, 270.
[39] A. Matthews, A. R. Lefkow, *Thin Solid Films* **1985**, *126*, 283.
[40] M. Wuttig, N. Yamada, *Nat. Mater.* **2007**, *6*, 824.
[41] T. Cao, C. W. Wei, R. E. Simpson, L. Zhang, M. J. Cryan, *Sci. Rep.* **2014**, *4*, 3955.
[42] C. Li, W. Zhu, Z. Liu, S. Yan, R. H. Pan, S. Du, J. J. Li, C. Z. Gu, *Appl. Phys. Lett.* **2018**, *113*, 231103.
[43] W. L. Luo, Z. Ji, S. H. Yang, D. Xing, *Phys. Rev. Appl.* **2018**, *10*, 024044.
[44] A. Tittl, A. K. U. Michel, M. Schaferling, X. H. Yin, B. Gholipour, L. Cui, M. Wuttig, T. Taubner, F. Neubrech, H. Giessen, *Adv. Mater.* **2015**, *27*, 4597.